© 2016. Published by The Company of Biologists Ltd | Development (2016) 143, 2753-2759 doi:10.1242/dev.128348

RESEARCH REPORT

IMP2 axonal localization, RNA interactome, and function in the development of axon trajectories

Nicolas Preitner[1,*], Jie Quan[1,*], Xinmin Li[1], Finn C. Nielsen[2] and John G. Flanagan[1,‡]

ABSTRACT

RNA-based regulatory mechanisms play important roles in the development and plasticity of neural circuits and neurological disease. Developing axons provide a model well suited to the study of RNA-based regulation, and contain specific subsets of mRNAs that are locally translated and have roles in axon pathfinding. However, the RNA-binding proteins involved in axon pathfinding, and their corresponding mRNA targets, are still largely unknown. Here we find that the RNA-binding protein IMP2 (Igf2bp2) is strikingly enriched in developing axon tracts, including in spinal commissural axons. We used the HITS-CLIP approach to perform a genome-wide identification of RNAs that interact directly with IMP2 in the native context of developing mouse brain. This IMP2 interactome was highly enriched for mRNA targets related to axon guidance. Accordingly, IMP2 knockdown in the developing spinal cord led to strong defects in commissural axon trajectories at the midline intermediate target. These results reveal a highly distinctive axonal enrichment of IMP2, show that it interacts with a network of axon guidance-related mRNAs, and reveal that it is required for normal axon pathfinding during vertebrate development.

KEY WORDS: IMP2, Igf2bp2, RNA interactome, RNA-binding protein, Axon guidance

INTRODUCTION

During neural development, axons must find their targets by navigating through pathways that may be long and complex (Dickson, 2002). Developing axons are highly specialized structures that express specific and dynamically regulated subsets of proteins. Although axonal proteins can be synthesized in the cell body and transported to the axon, specific subsets of proteins are synthesized locally from mRNAs within the axon. This local protein synthesis allows axons to autonomously regulate their structure and function, and is involved in spatially restricted responses such as growth cone turning, and the changes in axon responsiveness to guidance cues that occur at intermediate targets (Holt and Schuman, 2013).

RNA-binding proteins play key roles in regulating gene expression at the RNA level during normal development (Holt and Schuman, 2013), and many have been linked to human neurological diseases (Castello et al., 2013). However, only a few specific RNA-binding proteins have been studied in the context of neuron and axon development, and more generally the biological functions of most RNA-binding proteins remain little characterized (Hornberg and Holt, 2013). Among the best-studied is IMP1 (also known as Igf2bp1 or ZBP1), which binds to the 'zipcode' sequence in the 3′UTR of β-actin mRNA, and regulates β-actin mRNA transport and local translation in fibroblasts, neurons and other cell types (Kiebler and Bassell, 2006; Rodriguez et al., 2008; Gomes et al., 2014). A related member of the IMP family is IMP2 (also known as Igf2bp2), but its function is not well characterized and has only recently begun to emerge. Several studies have now identified roles for IMP2 in adult energy metabolism, obesity and type 2 diabetes (Christiansen et al., 2009; Dai et al., 2015). Additionally, studies have implicated IMP2 in the regulation of myogenesis (Li et al., 2012) and differentiation of neocortical neural precursor cells (Fujii et al., 2013).

Here we find that IMP2 protein distribution in the developing nervous system shows a highly distinctive enrichment in axon tracts. This prompted us to perform a genome-wide identification of RNA targets of IMP2 in the developing mouse nervous system using the HITS-CLIP technique, which allows identification of directly bound RNA targets in native tissues (Licatalosi et al., 2008; Darnell, 2013), and the results revealed an mRNA interactome highly enriched for functions related to axon development. Accordingly, in the well-characterized spinal commissural axon guidance model (Reeber and Kaprielian, 2009; Dickson and Zou, 2010; Nawabi and Castellani, 2011; Preitner et al., 2013; Kaplan et al., 2014), *in vivo* knockdown of IMP2 led to strong effects on axonal trajectories. Together, these results reveal a characteristic localization and function of IMP2 in axon pathfinding, identify an RNA interactome, and suggest that IMP2 might regulate a network of guidance-related mRNAs within the axon.

RESULTS AND DISCUSSION

IMP2 is enriched in developing axon tracts

We first investigated the expression patterns of the three members of the IMP family in developing mouse spinal cord by immunolabeling with previously characterized antibodies (Hammer et al., 2005). This analysis focused on dorsal spinal commissural neurons (Fig. 1A-C). IMP1 immunolabeling appeared ubiquitous in spinal cord (Fig. 1D,E), consistent with many previous studies showing that IMP1 has widespread roles in neurons and other cell types (Kiebler and Bassell, 2006; Rodriguez et al., 2008; Gomes et al., 2014). IMP3 (Igf2bp3), the family member most closely related to IMP1 in sequence, showed broad labeling comparable to IMP1 (Fig. 1H,I). IMP2 immunolabeling, by contrast, showed a highly distinctive preferential localization over axon tracts, including the ventral commissure and ventral funiculus (Fig. 1F,G) as well as other embryonic axon tracts (Fig. 1F,G; data not shown). The most prominent commissural axon signal was observed in the tracts where contralateral axon segments are bundled, but labeling was also visible in the ipsilateral axon

[1]Department of Cell Biology and Program in Neuroscience, Harvard Medical School, Boston, MA 02115, USA. [2]Center for Genomic Medicine, Rigshospitalet, University of Copenhagen, Blegdamsvej 9, Copenhagen Ø DK-2100, Denmark.
*These authors contributed equally to this work

‡Author for correspondence (flanagan@hms.harvard.edu)

J.G.F., 0000-0003-1341-1848

Received 5 August 2015; Accepted 13 June 2016

Development (2016) 143, 2753-2759 doi:10.1242/dev.128348

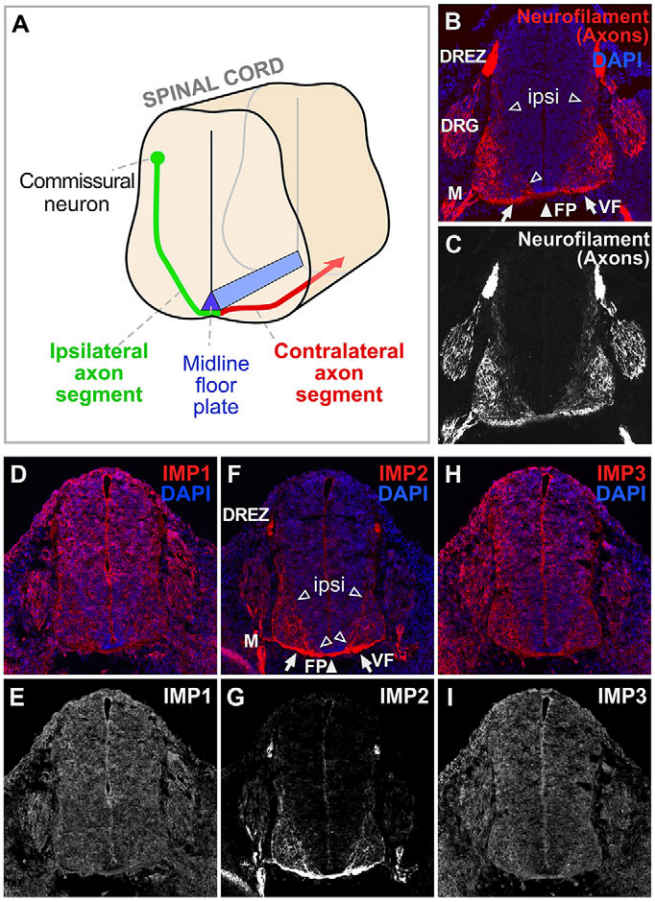

Fig. 1. IMP2 is highly enriched in axon tracts. (A) Diagram of axons of dorsal commissural neurons navigating in developing spinal cord. Axon segments on the ipsilateral side (green) orient ventrally and medially from the cell bodies toward the midline floor plate (blue). After crossing the floor plate in the ventral commissure, most axons make a sharp anterior turn, then diverge away from the midline, before growing longitudinally in the ventral and lateral funiculi. (B-I) Transverse sections of E11.5 mouse spinal cord, with DAPI nuclear staining in blue and immunolabeling in red. (B,C) Neurofilament marker for axons. (D,E) Consistent with previous studies, IMP1 labeling was seen broadly in the nervous system as well as in other tissues. (F,G) IMP2 labeling was seen over the ventral funiculus, the ventral commissure, and ipsilateral axon segments oriented towards the floor plate. (H,I) IMP3 labeling, similar to that of IMP1, was seen broadly in the nervous system and other tissues. ipsi, ipsilateral axon segments (open arrowheads); FP, floor plate (white arrowhead); VF, ventral funiculus (arrows); DRG, dorsal root ganglion; DREZ, dorsal root entry zone; M, spinal motor axons.

segments that follow less fasciculated trajectories toward the floor plate (Fig. 1F,G). Consistent with these results, a pan-IMP antibody gave essentially a composite of the three distributions, showing some generalized labeling together with strong labeling in commissural axons (data not shown). Given its striking distribution in axon tracts, we focused on IMP2 for further studies.

Identification of the IMP2 RNA interactome in brain by HITS-CLIP

To identify genome-wide RNA targets for IMP2 in brain, we used HITS-CLIP, which combines UV crosslinking and immunoprecipitation (CLIP) with high-throughput sequencing (Fig. 2A) (Licatalosi et al., 2008). Covalent UV crosslinking allows highly stringent washing to remove non-specific interactions, and has a very short range, thereby identifying directly interacting target RNAs. To reduce potential false positives, two different IMP2 antibodies were used, and two independent immunoprecipitation experiments were performed for each, giving a total of four data sets (Fig. S1A), in line with previous HITS-CLIP studies (see Preitner et al., 2014). IMP2 binding peaks were identified by a protocol that gives a low false discovery rate (FDR<0.001; see Fig. S1 and the supplementary Materials and Methods for details), resulting in the identification of 1850 high-confidence binding peaks in mRNAs from 747 genes (Table S1).

Fig. 2B shows examples of peak distribution for representative target mRNAs encoding proteins with known functions in axon development: Ncam1, Clasp1, Dcx and Robo2. Over 90% of the identified binding peaks were located in mRNA 3′UTRs (Fig. 2C), as is typical of many other regulatory RNA-binding proteins (Holt and Schuman, 2013). A consensus sequence was identified for IMP2 interaction (Fig. 2D, Fig. S2). This relatively short 7-8 nt sequence was found in only a fraction of targets (Fig. 2D, Fig. S2). These features are comparable to motifs associated with many other RNA-binding proteins (Anko and Neugebauer, 2012), and suggest that the motif is unlikely to be an obligate IMP2 binding consensus and might instead be associated with RNA secondary structure or the binding of accessory factors. Previously, IMP2 was used among a panel of several RNA-binding proteins to validate that the PAR-CLIP technique can detect protein-RNA interactions, resulting in identification of a shorter and highly degenerate 3-4 nt motif (Hafner et al., 2010); that a different motif was observed could reflect the use of overexpressed recombinant IMP2 in HEK 293 cells (Bell et al., 2013). The HITS-CLIP approach used here examined RNAs associated with endogenously expressed IMP2 in the native context of developing brain. We next used bioinformatic tools to assess the functions of the identified targets.

Global functional analysis of brain IMP2 target mRNAs

First, the Ingenuity Pathway Analysis (IPA) package was used to detect enriched signaling pathways. The top canonical signaling category was axon guidance signaling, with strong enrichment and a highly significant *P*-value (Fig. 3A). The next four categories were related to specific axon guidance cues, namely the ephrins and semaphorins, followed by Rho GTPase signaling, which also plays important roles in cell migration and axon guidance. We also performed a Gene Ontology (GO) analysis using the DAVID bioinformatics platform and, very consistent with the IPA analysis, the most enriched functions were related to cell migration, axon and neuron morphogenesis, and cytoskeleton organization (Fig. 3B). Although the use of brain as a source clearly selects for brain-related functions, the analysis used the E14 brain transcriptome as background, and considering that many neurodevelopmental processes are occurring in the brain at that stage, the enrichment of functions related to axon migration was robust and highly significant.

Since our localization experiments revealed enrichment of IMP2 in axon tracts (Fig. 1), we compared IMP2 targets with known axonally localized mRNAs. Strong overlap was observed between a list of axonally localized mRNAs (Gumy et al., 2011) and IMP2 target mRNAs (37% of IMP2 targets; $P<10^{-15}$; Fig. 3C). This result seems very consistent with a model in which IMP2 regulates mRNAs locally within the axon.

In addition to biological functions, we were also interested in disease associations. IPA Disease and Disorder Analysis showed that neurological disease was the most significantly enriched category, including enrichment of multiple neurological disease subcategories (Fig. S3). Moreover, 112 of the IMP2 target mRNAs

Development (2016) 143, 2753-2759 doi:10.1242/dev.128348

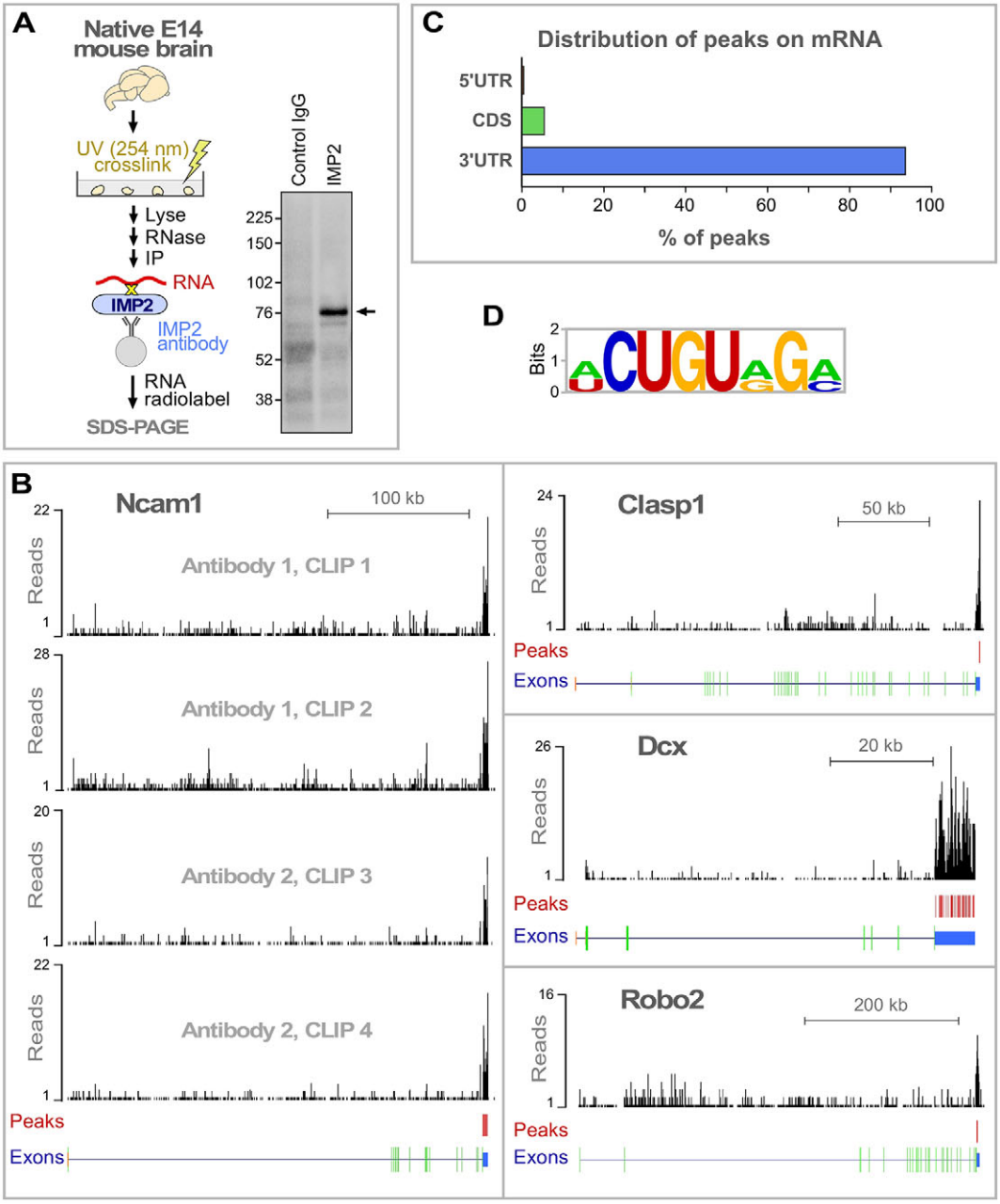

Fig. 2. HITS-CLIP identification of RNAs that interact with IMP2. (A) IMP2 HITS-CLIP. After UV-crosslinking protein-RNA complexes in native E14 mouse brain tissue, radiolabeled RNAs were co-immunoprecipitated with IMP2. CLIP results are shown on the right. Arrow marks the major band with increased intensity in the experimental lane, at the size expected for IMP2-RNA complexes, which was taken for high-throughput sequencing. Molecular mass markers in kDa. (B) Distribution of IMP2 HITS-CLIP sequence signals on representative target genes. Red vertical bars indicate high-confidence IMP2 binding peaks (see Fig. S1A and the supplementary Materials and Methods for details on peak identification). Structure of each gene is illustrated beneath: 5′UTR, orange; protein-coding, green; 3′UTR, blue. (C) Distribution of IMP2 binding peaks on target mRNAs. CDS, coding sequence. (D) A consensus sequence motif identified within the IMP2 binding regions using MEME software (see also Fig. S2).

correspond to genes responsible for human Mendelian diseases (Table S2). The significant association with Alzheimer's disease is especially intriguing, given that IMP2 is also associated with type 2 diabetes (Scott et al., 2007; Zeggini et al., 2007; Saxena et al., 2007; Lyssenko et al., 2008): type 2 diabetes is a risk factor for Alzheimer's disease (Haan, 2006; Li et al., 2007) and pathological processes such as insulin resistance underlie both conditions (Li et al., 2007; Kim and Feldman, 2012). This suggests the intriguing possibility that IMP2 might provide a molecular link between type 2 diabetes and Alzheimer's disease by regulating targets such as insulin receptor mRNA or other mRNAs in its interactome that are related to both diabetes and neurodegeneration.

IMP2 is required for normal commissural axon trajectories *in vivo*

Since our studies of the IMP2 expression pattern and mRNA interactome strongly pointed to a role in axon development, we next performed experiments on commissural axon guidance *in vivo*. Commissural axon trajectories are described in Fig. 1A. In terms of molecular guidance mechanisms, initial growth toward the midline

Development (2016) 143, 2753-2759 doi:10.1242/dev.128348

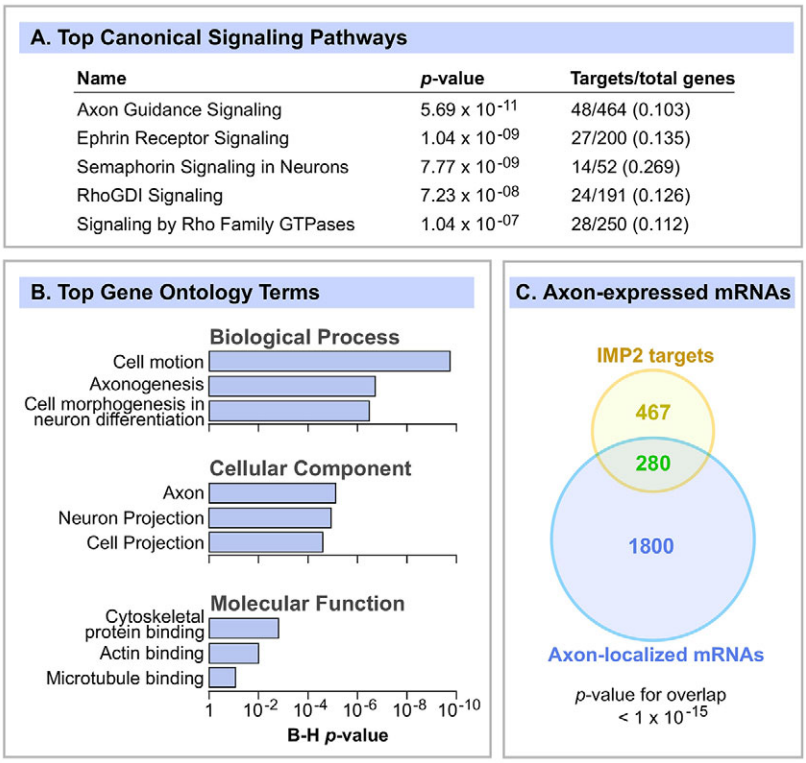

Fig. 3. IMP2 target mRNAs are highly enriched for functions related to axon development. (A) IMP2 target mRNAs were analyzed by IPA to identify enriched canonical signaling pathways, of which the top five are shown. Right-hand column shows target genes as a fraction of the total number of genes in the IPA category. (B) The top GO terms enriched among IMP2 target mRNAs, identified by the DAVID bioinformatic tools. *P*-values were adjusted for multiple comparisons by the Benjamini-Hochberg (B-H) method. (C) Venn diagram comparing IMP2 target mRNAs with a catalog of axon-localized mRNAs in embryonic mouse DRG axons (Gumy et al., 2011). Statistics used Fisher's exact test.

is mediated by floor plate attractants. Since the floor plate is an intermediate target, after crossing the axons must undergo a drastic 'midline switch' in responsiveness to cues, losing their responsiveness to midline attractants and becoming sensitive instead to midline repellents including Slits. In addition to ensuring that axons do not recross, this switch also renders the axons responsive to cues that guide their post-crossing trajectories, including anteroposterior guidance gradients, and divergence away from the midline due to Slit-mediated repulsion.

Spinal cords of chick embryos *in ovo* were electroporated 1-2 days before commissural axons reach the floor plate, unilaterally with plasmids encoding IMP2-specific shRNAs or control shRNA, along with GFP under control of the *Math1* (*Atoh1*) promoter to trace commissural axons (Helms and Johnson, 1998; Lumpkin et al., 2003; Reeber et al., 2008). Commissural axon trajectories were then visualized 64 h later (E5.5, HH stage 24-25) in spinal cord open-book preparations. In embryos treated with control shRNA at this stage, most axons have crossed the midline (Fig. 4B,E). By contrast, in embryos subjected to IMP2 shRNAs, a much lower proportion of axons had crossed to the contralateral side, and instead many growth cones were observed at or near the ipsilateral side of the floor plate, where they had the typical morphology of stalled growth cones (Fig. 4C, arrowheads; see also Fig. 4E,F and left panel of 4D). Similar phenotypes were observed using two different shRNAs that knock down IMP2 (Fig. 4E,F, Fig. S4A). Interestingly, in the IMP2 RNAi embryos, for those axons that progressed beyond the initial encounter with the floor plate, approximately half turned contralaterally and half turned ipsilaterally (Fig. 4D, right panel, orange and red trajectories in the diagram), in contrast to the classical contralateral trajectory (red trajectory in Fig. 4A). These aberrant ipsilateral trajectories approximately mirrored the contralateral trajectories, turning anteriorly and away from the midline (Fig. 4D, right panel and diagram).

The observation that IMP2 RNAi leads to frequent stalling of commissural axons at the midline is intriguing because this phenotype is strikingly similar to the loss-of-function phenotype of one of the IMP2 targets, Robo1, in both mouse and chick embryos (Long et al., 2004; Philipp et al., 2012). Robo1 is a receptor for the midline repellent Slit, and this receptor is upregulated on commissural axons upon reaching the midline, and enables commissural axons to escape the midline. To test whether IMP2 might be involved in the expression of Robo1, we performed IMP2 RNAi *in ovo*, and then cultured commissural neurons for analysis of Robo1 protein levels in axons and cell bodies. The results showed that IMP2 knockdown reduced Robo1 immunolabeling in axons but not in the cell body (Fig. 4G), providing functional evidence that axonal Robo1 expression is downstream of IMP2.

Our observations that IMP2 labeling is strongly enriched in axon tracts, that it binds mRNAs highly enriched for functions in axon guidance, and that knockdown leads to strong defects in axon trajectories *in vivo*, provide consistent evidence for a role of IMP2 in axon development. The enrichment of a large number of axon guidance-related mRNA targets in the IMP2 interactome suggests that it might coordinately regulate a broad RNA program for axon development. This could entail binding a large number of mRNAs within individual neurons or, alternatively, a smaller subset of mRNAs in multiple diverse neuron types. The enrichment of IMP2 in axon tracts is particularly interesting; indeed, we do not know of any other mammalian RNA-binding protein that has been described to show such a distinctive enrichment in developing axon tracts, and our data suggest a model whereby IMP2 regulates mRNAs locally within the axon.

Regarding a mechanistic explanation for the observed effect of IMP2 knockdown on commissural axon development, one model is that IMP2 could be required for the expression of a general program of mRNAs needed for axon growth and guidance. However, after IMP2 knockdown, axons initially grew toward the floor plate

Development (2016) 143, 2753-2759 doi:10.1242/dev.128348

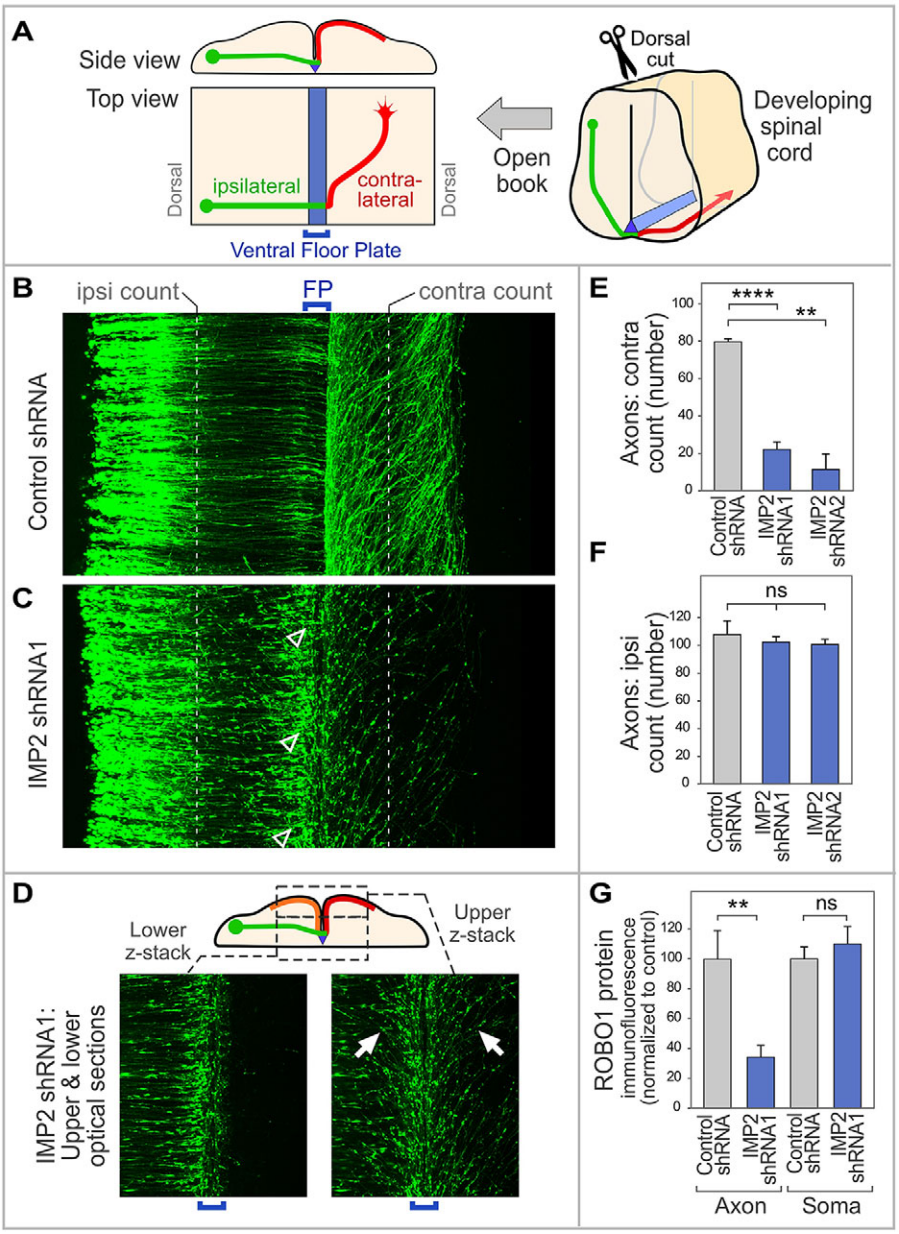

Fig. 4. IMP2 knockdown causes defects in commissural axon pathfinding *in vivo*. (A) Diagram of spinal cord open-book preparation. The developing spinal cord is cut open along the dorsal midline, then mounted ventricular face downwards. A typical commissural axon ipsilateral segment (green), contralateral segment (red) and the floor plate (blue) are shown. (B-F) IMP2 or control shRNAs were introduced by *in ovo* electroporation into one side of the chick embryo spinal cord, with a Math1-GFP construct to trace commissural axons. Spinal cord was dissected 64 h later and imaged as an open-book. (B) Commissural axons in a confocal *z*-stack of open-book, viewed from the top. Electroporated cell bodies are visible on the left, and axons grow toward the right. (C) After IMP2 knockdown, in contrast to the control many growth cones are seen to have stalled at or near the ipsilateral side of the floor plate, showing an enlarged fusiform morphology typical of stalled growth cones (arrowheads). Correspondingly, a reduced number of axons was seen on the contralateral side, where they appeared to follow roughly normal trajectories without obvious signs of degeneration. (D) The lower confocal *z*-stack shows axon segments approaching the floor plate (green in diagram). The upper *z*-stack shows axon trajectories diverging away from the midline on both sides (contralateral, red in diagram; and ipsilateral, orange in diagram; examples of the approximately mirror image trajectories are arrowed). (E,F) Quantitation of ipsilateral and contralateral axon numbers, counted at the positions indicated by the white dashed lines in B and C. IMP2 knockdown did not significantly affect the number of axons emerging from the dorsal commissural neuron cell bodies and growing toward the floor plate, but strongly reduced the percentage of axons on the contralateral side. Each replicate was a separate embryo. (G) Effect of IMP2 RNAi on Robo1 expression in spinal commissural neurons. IMP2 or control shRNAs were introduced by *in ovo* electroporation into chick embryo spinal cord, with a Math1-GFP construct to identify transfected neurons; 64 h later, commissural neurons were dissociated and cultured for analysis of Robo1 immunofluorescence in axons and cell bodies. Immunolabeling was performed on permeabilized cells to detect both intracellular and cell surface Robo1. IMP2 shRNA reduced Robo1 expression in the axon, but not in the soma (see also Fig. S4B). Each replicate in this experiment was a different neuron (n=16 for control and n=28 for IMP2 shRNA), and the experiment was repeated three times to ensure reproducibility. Comparisons used Student's unpaired two-tailed t-test. Error bars show s.e.m. **P<0.01, ****P<0.0001; ns, not significant.

without obvious abnormalities, and then showed highly specific phenotypes near the midline, including both stalling and mirror trajectories. These observations suggest a more specific model whereby IMP2 participates in the midline switch of axon behavior. In this latter scenario, IMP2 might first be involved in the transport of mRNAs into the axon, and then the regulation of IMP2 function

Development (2016) 143, 2753-2759 doi:10.1242/dev.128348

by a presumptive midline signal could initiate a program of mRNA translation in post-crossing axon segments. Indeed, multiple proteins, including Robo receptors, are known to be upregulated in post-crossing axon segments, and translational control mechanisms within the axon can provide a mechanism for this regulation (Brittis et al., 2002; Colak et al., 2013; Preitner et al., 2013). Also potentially consistent with this model is the identification, among the IMP2 targets, of Robo1, a receptor for the midline repellent Slit, which produces a loss-of-function phenotype of stalling at the midline (Brose et al., 1999; Long et al., 2004; Jaworski et al., 2010; Philipp et al., 2012) comparable to the strong stalling phenotype seen here in the IMP2 loss-of-function analysis. These observations also fit with the prominent expression of both IMP2 and Robo1 in commissural axons, as well as our finding that axonal Robo1 expression is reduced by IMP2 loss-of-function. Together, these findings lead to a model in which IMP2 regulation of Robo1 contributes to the midline switch. IMP2 regulation of other targets might also contribute, since our CLIP list includes mRNAs for additional proteins involved in axon growth and guidance, including some known to have midline guidance phenotypes. Moreover, RNA-based mechanisms of the type studied here (Brittis et al., 2002; Colak et al., 2013; Preitner et al., 2013) are likely to act in concert with switch mechanisms at other molecular levels (Nawabi and Castellani, 2011; Neuhaus-Follini and Bashaw, 2015; Alther et al., 2016) to accomplish this complex biological process.

In connection with a possible role of IMP2 in the midline switch, it is intriguing that IMP1 phosphorylation upregulates translation of its target β-actin mRNA (Rodriguez et al., 2008), and it seems conceivable that IMP2 might undergo a similar form of regulation by signals at the midline. Further studies would be required to investigate specific molecular mechanisms that might lead to the regulated action of IMP2 in axons. Also, although other genes that cause strong commissural axon crossing phenotypes do not necessarily produce obvious behavioral defects in mice, it would be interesting to determine whether *Imp2* gene knockout mice (Dai et al., 2015) have behavioral phenotypes, as this has not yet been characterized.

In conclusion, it has been appreciated for well over a decade that RNA-based regulation plays important and unique roles in axon development, but little is known about the RNA-binding proteins involved, or their RNA targets. By genome-wide identification of target mRNAs for IMP2 in a native physiological context, namely the developing brain, we find strong enrichment for targets involved in axon growth and guidance. Taken together with the striking localization of IMP2 in developing axon tracts, and the strong functional effects of IMP2 loss-of-function on axon trajectories *in vivo*, these results identify novel roles of IMP2 in axon development, and now open the door to further studies into the mechanistic basis of RNA-based processes in the axon.

MATERIALS AND METHODS

Immunolabeling

Immunolocalization of IMP1-3 in mouse E11.5 spinal cord sections was performed as described in the supplementary Materials and Methods. All animal experiments were performed in compliance with relevant ethical regulations, and were approved by the IACUC at Harvard Medical School.

HITS-CLIP

HITS-CLIP, RNA-seq and associated bioinformatic analysis (including peak identification, motif searching, GO, IPA) were performed as previously described (Preitner et al., 2014), except as noted in the supplementary Materials and Methods.

In ovo electroporation

In ovo electroporation in chicken embryos was performed essentially as described (Reeber et al., 2008). Fertilized eggs (Charles River Laboratories) were incubated 38°C for 64 h. A DNA mix containing shRNA and EGFP plasmid with Trypan Blue dye was introduced with a glass micropipette into the spinal cord lumen of HH stage 17 embryos and unilaterally electroporated. Windowed eggs were further incubated at 37°C for 64 h, then mounted as open-books and imaged by confocal microscopy. Details of the shRNA constructs and electroporation procedures are provided in the supplementary Materials and Methods.

Acknowledgements

We thank Jane Johnson for sharing the *Math1* plasmid; Jiangwen Zhang, Christian Daly and the Bauer Center for Genomic Research for support with deep sequencing; and Jennifer Waters and the Nikon Imaging Center at Harvard Medical School for imaging equipment and expertise.

Competing interests

The authors declare no competing or financial interests.

Author contributions

N.P. designed the study and participated in all experiments. J.Q. participated in the RNAi experiments and performed the bioinformatic analysis. X.L. participated in the RNAi experiments, made the Math1-GFP construct and participated in methods development for the *in vivo* experiments. F.C.N. provided IMP antibodies and consulted on the project. J.G.F. supervised the study, and designed and analyzed it with the other authors. J.Q., N.P. and J.G.F. wrote the manuscript.

Funding

This work was supported by grants from the National Institutes of Health [R01 NS069913, R37 HD029417, R01 EY011559] and a fellowship from the Charles A. King Trust (to N.P.). Deposited in PMC for release after 12 months.

Data availability

HITS-CLIP data have been deposited at NCBI Gene Expression Omnibus and are accessible through GEO Series accession number GSE83822 (http://www.ncbi.nlm.nih.gov/geo/query/acc.cgi?acc=GSE83822).

Supplementary information

Supplementary information available online at
http://dev.biologists.org/lookup/doi/10.1242/dev.128348.supplemental

References

Alther, T. A., Domanitskaya, E. and Stoeckli, E. T. (2016). Calsyntenin 1-mediated trafficking of axon guidance receptors regulates the switch in axonal responsiveness at a choice point. *Development* **143**, 994-1004.

Änkö, M.-L. and Neugebauer, K. M. (2012). RNA-protein interactions in vivo: global gets specific. *Trends Biochem. Sci.* **37**, 255-262.

Bell, J. L., Wächter, K., Mühleck, B., Pazaitis, N., Köhn, M., Lederer, M. and Hüttelmaier, S. (2013). Insulin-like growth factor 2 mRNA-binding proteins (IGF2BPs): post-transcriptional drivers of cancer progression? *Cell. Mol. Life Sci.* **70**, 2657-2675.

Brittis, P. A., Lu, Q. and Flanagan, J. G. (2002). Axonal protein synthesis provides a mechanism for localized regulation at an intermediate target. *Cell* **110**, 223-235.

Brose, K., Bland, K. S., Wang, K. H., Arnott, D., Henzel, W., Goodman, C. S., Tessier-Lavigne, M. and Kidd, T. (1999). Slit proteins bind robo receptors and have an evolutionarily conserved role in repulsive axon guidance. *Cell* **96**, 795-806.

Castello, A., Fischer, B., Hentze, M. and Preiss, T. (2013). RNA-binding proteins in Mendelian disease. *Trends Genet.* **29**, 318-327.

Christiansen, J., Kolte, A. M., Hansen, T. V. O. and Nielsen, F. C. (2009). IGF2 mRNA-binding protein 2: biological function and putative role in type 2 diabetes. *J. Mol. Endocrinol.* **43**, 187-195.

Colak, D., Ji, S. J., Porse, B. T. and Jaffrey, S. R. (2013). Regulation of axon guidance by nonsense-mediated mRNA decay. *Cell* **153**, 1252-1265.

Dai, N., Zhao, L., Wrighting, D., Krämer, D., Majithia, A., Wang, Y., Cracan, V., Borges-Rivera, D., Mootha, V. K., Nahrendorf, M. et al. (2015). IGF2BP2/IMP2-Deficient mice resist obesity through enhanced translation of Ucp1 mRNA and Other mRNAs encoding mitochondrial proteins. *Cell Metab.* **21**, 609-621.

Darnell, R. B. (2013). RNA protein interaction in neurons. *Annu. Rev. Neurosci.* **36**, 243-270.

Dickson, B. J. (2002). Molecular mechanisms of axon guidance. *Science* **298**, 1959-1964.

Dickson, B. J. and Zou, Y. (2010). Navigating intermediate targets: the nervous system midline. *Cold Spring Harb. Perspect. Biol.* **2**, a002055.

Development (2016) 143, 2753-2759 doi:10.1242/dev.128348

Fujii, Y., Kishi, Y. and Gotoh, Y. (2013). IMP2 regulates differentiation potentials of mouse neocortical neural precursor cells. *Genes Cells* **18**, 79-89.

Gomes, C., Merianda, T. T., Lee, S. J., Yoo, S. and Twiss, J. L. (2014). Molecular determinants of the axonal mRNA transcriptome. *Dev. Neurobiol.* **74**, 218-232.

Gumy, L. F., Yeo, G. S., Tung, Y.-C. L., Zivraj, K. H., Willis, D., Coppola, G., Lam, B. Y. H., Twiss, J. L., Holt, C. E. and Fawcett, J. W. (2011). Transcriptome analysis of embryonic and adult sensory axons reveals changes in mRNA repertoire localization. *RNA* **17**, 85-98.

Haan, M. N. (2006). Therapy Insight: type 2 diabetes mellitus and the risk of late-onset Alzheimer's disease. *Nat. Clin. Pract. Neurol.* **2**, 159-166.

Hafner, M., Landthaler, M., Burger, L., Khorshid, M., Hausser, J., Berninger, P., Rothballer, A., Ascano, M., Jungkamp, A.-C., Munschauer, M. et al. (2010). Transcriptome-wide identification of RNA-binding protein and microRNA target sites by PAR-CLIP. *Cell* **141**, 129-141.

Hammer, N. A., Hansen, T. V. O., Byskov, A. G., Rajpert-De Meyts, E., Grondahl, M. L., Bredkjaer, H. E., Wewer, U. M., Christiansen, J. and Nielsen, F. C. (2005). Expression of IGF-II mRNA-binding proteins (IMPs) in gonads and testicular cancer. *Reproduction* **130**, 203-212.

Helms, A. and Johnson, J. (1998). Progenitors of dorsal commissural interneurons are defined by MATH1 expression. *Development* **125**, 919-928.

Holt, C. E. and Schuman, E. M. (2013). The central dogma decentralized: new perspectives on RNA function and local translation in neurons. *Neuron* **80**, 648-657.

Hörnberg, H. and Holt, C. (2013). RNA-binding proteins and translational regulation in axons and growth cones. *Front. Neurosci.* **7**, 81.

Jaworski, A., Long, H. and Tessier-Lavigne, M. (2010). Collaborative and specialized functions of Robo1 and Robo2 in spinal commissural axon guidance. *J. Neurosci.* **30**, 9445-9453.

Kaplan, A., Kent, C. B., Charron, F. and Fournier, A. E. (2014). Switching responses: spatial and temporal regulators of axon guidance. *Mol. Neurobiol.* **49**, 1077-1086.

Kiebler, M. A. and Bassell, G. J. (2006). Neuronal RNA granules: movers and makers. *Neuron* **51**, 685-690.

Kim, B. and Feldman, E. L. (2012). Insulin resistance in the nervous system. *Trends Endocrinol. Metab.* **23**, 133-141.

Li, L. and Holscher, C. (2007). Common pathological processes in Alzheimer disease and type 2 diabetes: a review. *Brain Res. Rev.* **56**, 384-402.

Li, Z., Gilbert, J. A., Zhang, Y., Zhang, M., Qiu, Q., Ramanujan, K., Shavlakadze, T., Eash, J. K., Scaramozza, A., Goddeeris, M. M. et al. (2012). An HMGA2-IGF2BP2 axis regulates myoblast proliferation and myogenesis. *Dev. Cell* **23**, 1176-1188.

Licatalosi, D. D., Mele, A., Fak, J. J., Ule, J., Kayikci, M., Chi, S. W., Clark, T. A., Schweitzer, A. C., Blume, J. E., Wang, X. et al. (2008). HITS-CLIP yields genome-wide insights into brain alternative RNA processing. *Nature* **456**, 464-469.

Long, H., Sabatier, C., Ma, L., Plump, A., Yuan, W., Ornitz, D. M., Tamada, A., Murakami, F., Goodman, C. S. and Tessier-Lavigne, M. (2004). Conserved roles for Slit and Robo proteins in midline commissural axon guidance. *Neuron* **42**, 213-223.

Lumpkin, E. A., Collisson, T., Parab, P., Omer-Abdalla, A., Haeberle, H., Chen, P., Doetzlhofer, A., White, P., Groves, A., Segil, N. et al. (2003). Math1-driven GFP expression in the developing nervous system of transgenic mice. *Gene Expr. Patterns* **3**, 389-395.

Lyssenko, V., Jonsson, A., Almgren, P., Pulizzi, N., Isomaa, B., Tuomi, T., Berglund, G., Altshuler, D., Nilsson, P. and Groop, L. (2008). Clinical risk factors, DNA variants, and the development of type 2 diabetes. *N. Engl. J. Med.* **359**, 2220-2232.

Nawabi, H. and Castellani, V. (2011). Axonal commissures in the central nervous system: how to cross the midline? *Cell. Mol. Life Sci.* **68**, 2539-2553.

Neuhaus-Follini, A. and Bashaw, G. J. (2015). Crossing the embryonic midline: molecular mechanisms regulating axon responsiveness at an intermediate target. *Wiley Interdiscip. Rev. Dev. Biol.* **4**, 377-389.

Philipp, M., Niederkofler, V., Debrunner, M., Alther, T., Kunz, B. and Stoeckli, E. T. (2012). RabGDI controls axonal midline crossing by regulating Robo1 surface expression. *Neural Dev.* **7**, 36.

Preitner, N., Quan, J. and Flanagan, J. G. (2013). This message will self-destruct: NMD regulates axon guidance. *Cell* **153**, 1185-1187.

Preitner, N., Quan, J., Nowakowski, D. W., Hancock, M. L., Shi, J., Tcherkezian, J., Young-Pearse, T. L. and Flanagan, J. G. (2014). APC is an RNA-binding protein, and its interactome provides a link to neural development and microtubule assembly. *Cell* **158**, 368-382.

Reeber, S. L. and Kaprielian, Z. (2009). Leaving the midline: how Robo receptors regulate the guidance of post-crossing spinal commissural axons. *Cell Adh. Migr.* **3**, 300-304.

Reeber, S. L., Sakai, N., Nakada, Y., Dumas, J., Dobrenis, K., Johnson, J. E. and Kaprielian, Z. (2008). Manipulating Robo expression in vivo perturbs commissural axon pathfinding in the chick spinal cord. *J. Neurosci.* **28**, 8698-8708.

Rodriguez, A. J., Czaplinski, K., Condeelis, J. S. and Singer, R. H. (2008). Mechanisms and cellular roles of local protein synthesis in mammalian cells. *Curr. Opin. Cell Biol.* **20**, 144-149.

Saxena, R., Voight, B., Lyssenko, V., Burtt, N. l., de Bakker, P., Chen, H., Roix, J., Kathiresan, S., Hirschhorn, J., Daly, M. et al. (2007). Genome-wide association analysis identifies loci for type 2 diabetes and triglyceride levels. *Science* **316**, 1331-1336.

Scott, L., Mohlke, K., Bonnycastle, L., Willer, C., Li, Y., Duren, W., Erdos, M., Stringham, H., Chines, P., Jackson, A. et al. (2007). A genome-wide association study of type 2 diabetes in Finns detects multiple susceptibility variants. *Science* **316**, 1341-1345.

Zeggini, E., Weedon, M., Lindgren, C., Frayling, T., Elliott, K., Lango, H., Timpson, N., Perry, J., Rayner, N., Freathy, R. et al. (2007). Replication of genome-wide association signals in UK samples reveals risk loci for type 2 diabetes. *Science* **316**, 1336-1341.

SUPPLEMENTARY MATERIALS AND METHODS

HITS-CLIP and RNA-seq

HITS-CLIP was performed essentially as described previously (Licatalosi et al., 2008; Preitner et al., 2014) on E14 Swiss Webster mouse brains. Briefly, embryonic brain tissues were partially dissociated before UV irradiation (UV at 254 nm, 3X 300 mJ/cm2 in a Stratalinker). Cell lysates were sonicated, treated with DNase, and digested with benzonase (Sigma E8263; at a final dilution of 1:2000; 10 min at 37°C) to produce protein-bound RNAs of ~40 nt fragments. Then pre-cleared lysates were mixed with 30 µl Sepharose beads and 30 µg antibody (mouse polyclonal anti-IMP2 antibody, Abnova H00010644-A01; rabbit anti-IMP2 antibody, Proteintech 11601-1-AP), and rotated for 3 hours at 4°C. Immunoprecipitated protein-RNA complexes were stringently washed with SDS- containing buffer and dephosphorylated, and the radiolabeled RNA adapter (5'-UCGUAUGCCGUCUUCUGCUUGU-3') were ligated at the 3' end of the RNA fragments. Protein-RNA complexes were then phosphorylated at the 5' end, separated on a 4-12% denaturing NuPAGE gel (Invitrogen), transferred to a nitrocellulose membrane, and exposed on a film. Narrow bands corresponding to the size of the specific protein-RNA complexes were then excised from the membrane. RNA fragments were extracted, ligated to the 5' adapter (5'-GUUCAGAGUUCUACAGUCCGACGAUC-3') and amplified by RT-PCR (primers: AATGATACGGCGACCACCGACAGGTTCAGAGTTCTACAGTCCGA, and CAAGCAGAAGACGGCATACGA). The purified PCR products were sequenced on Illumina sequencing platform.

For mRNA-seq, polyadenylated RNAs from E14 mouse brains were isolated, fragmented with benzonase, and ~40 nt RNA fragments isolated on a polyacrylamide gel. RNA fragments were dephosphorylated, 3' linkers were ligated, RNA fragments were gel isolated again,

rephosophorylated with polynucleotide kinase, and 5' linkers were added, before cDNA amplification, libary preparation, and sequencing in the same way as for CLIP.

Processing and alignment of HITS-CLIP reads

The quality of raw sequence reads (36 nt) was analyzed using fastQC (http://www.bioinformatics.babraham.ac.uk/projects/fastqc/). Adapter sequences were trimmed, and reads with more than 2 undetermined bases (Ns) were removed. The sum of base Phred quality scores of each read was calculated, and reads with the lowest 1% sum of Phred scores were filtered. The rest reads were trimmed from the 3'- end to retain 28 nt of high quality. After filtering and trimming, reads were aligned to mouse genome (NCBI37/mm9 assembly) using Bowtie (Langmead et al., 2009) (http://bowtie-bio.sourceforge.net/index.shtml), allowing up to 2 mismatches. Reads aligned to multiple positions in the genome were filtered. RefSeq mRNA database was used to build the exon junction index to align reads that overlap the exon junction sites. Those reads that were not aligned to genome were aligned to exon junctions, and only uniquely aligned reads were retained. Reads that aligned to the same genomic locations were collapsed to remove potential duplicates resulting from PCR amplifications. The control mRNA-seq data were aligned to the mouse genome and exon junction sites by the same procedure. The aligned reads were annotated based on RefSeq mRNA database. The distribution of reads in mouse genome was visualized on UCSC genome browser.

HITS-CLIP data have been deposited at NCBI Gene Expression Omnibus, and are accessible through GEO Series accession number GSE83822 (http://www.ncbi.nlm.nih.gov/geo/query/acc.cgi?acc=GSE83822).

Peak identification

To identify IMP2 binding sites, we next combined and analyzed reads from all four CLIP replicates. Overlapping reads were grouped into clusters, and each cluster was assigned two values, peak height and fold change. Peak height was defined as the maximum number of overlapping reads in the cluster, and median fold change was calculated by comparing to the randomly sampled background from mRNA-seq data. To differentiate significantly enriched IMP2 binding sites from false positives, we generated mock CLIP data sets by randomly sampling the same number of sequence reads as in the IMP2 CLIP samples from the control mRNA-seq data. The false discovery rate was calculated as the ratio of the number of peaks identified from mock CLIP data to that from CLIP data using the same cutoff. We selected high-confidence peaks on mature mRNAs, based on the following criteria: (a) a minimal peak height of 18 in pooled CLIP samples, which is greater than the maximal peak height in five different sets of mock CLIPs, (b) a minimal median fold change of 2, (c) reproducible peaks requiring that within a peak region, at least 4 overlapping reads be present in the four replicates. Additionally, in order to eliminate occasional mRNAs with high read coverage along the transcript but no prominent peaks, we required that the peak height should be at least 1.2x the highest peak in the introns, and at least 10x the average read coverage in the introns. The 1850 identified IMP2 binding sites mapped to 747 protein-coding genes (from RefSeq database).

Motif searching

Motif analysis was performed using MEME tools (Bailey et al., 2009) (http://meme.nbcr.net/meme/). The sequence logos were generated on WebLogo 2.8.2 (http://weblogo.berkeley.edu). The *Z*-score statistic for motif finding was applied as described (Tompa, 1999).

GO analysis of target mRNAs

The enrichment of gene ontology (GO) terms in IMP2 target mRNAs was analyzed using DAVID online tools (Huang et al., 2009) (http://david.abcc.ncifcrf.gov). Transcript abundance was determined from mRNA-seq data, and transcripts were considered as expressed if the lower bound of the 95% confidence interval of the estimated fragments per kilobase of exon model per million mapped fragments (FPKM) was greater than 0.1 (Trapnell et al., 2010) (http://cufflinks.cbcb.umd.edu). DAVID reported *p*-values, based on a modified Fisher's exact test. The *p*-values reported for this study were adjusted using the Benjamini-Hochberg method.

Functional analysis using IPA

Canonical pathway analysis, disease association, and network analysis were performed using the core analysis module of the Ingenuity Pathway Analysis (IPA) package. Figure 3D shows disorders corresponding to a specific disease and represented by at least two genes, within the IPA neurological disease category. Single genes causing human Mendelian disorders (Table S2) were identified by a systematic manual search in the OMIM database (http://www.ncbi.nlm.nih.gov/omim).

Comparison of IMP2 targets with axonally localized mRNAs

IMP2 target mRNAs were compared to the axonal mRNA list identified in rat dorsal root ganglion (Gumy et al., 2011). The two lists of mRNAs expressed in embryonic axons and adult axons were combined, and the Entrez Gene IDs and official symbols converted from Affymetrix ID were used for the comparison. The overlap between the target set and the axonal mRNAs was evaluated by Fisher's exact test. Venn diagram was drawn to scale using Venn diagram generator available online (http://jura.wi.mit.edu/bioc/tools/venn.php).

Immunolocalization in embryos

Cryostat sections (10 µm) were collected on Superfrost Plus slides (Fisher) and kept at -80°C. Slides were blocked in 1X PBS with 10% normal serum and 0.1% Triton X-100 for 30 min at room temperature (RT), incubated overnight at 4°C with the primary antibody diluted in the blocking solution, washed with PBS, incubated for 1 hour at RT with Alexa Fluor conjugated secondary antibody (Molecular Probes, 1:500) diluted in PBS with 10% normal serum, counterstained with DAPI, washed with PBS, and mounted using Fluoromount G mounting medium (SouthernBiotech). Primary antibodies and dilutions: anti-GFP antibody, Molecular Probes A11120, 1:200; anti-IMP1 antibody, 1:400 anti-IMP2 antibody, 1:1000; anti-IMP3 antibody, 1:1000 anti-neurofilament antibody, Sigma N5264, 1:400). IMP1, 2, and 3 antibodies were obtained from Finn C Nielsen's lab at University of Copenhagen in Denmark. Images were captured using a Nikon 80i upright fluorescence microscope.

DNA constructs for RNAi experiments

Plasmids expressing IMP2 shRNAs were produced by cloning the following sequences under the U6 promoter (sense IMP2 target sequence underlined). As a control for RNAi experiments, a plasmid expressing a non-targeting control shRNA under the U6 promoter was used (based on the HuSH plasmid, Origene, and computationally confirmed not to recognize sequences in the chick transcriptome).

IMP2 shRNA1: GATCCACGGAACAGTGGAGAATGTGAAGCTTGA

CATTCTCCACTGTTCCGTTTTTTTGGAAGC

IMP2 shRNA2: GATCCGGACCTTAATGCCTTCAGAGAAGCTTGT

CTGAAGGCATTAAGGTCCTTTTTTGGAAGC

Control shRNA: GATCCACAAGATGAAGAGCACCAAGAAGCTTG

TTGGTGCTCTTCATCTTGT TTTTTTTGGAAGC

To test the effectiveness and specificity of shRNAs against IMP2, coding sequence constructs of IMP2 mRNA, and also IMP1 and IMP3 as controls, were first amplified by PCR from chick E5 spinal cord cDNA using the oligos shown below, and cloned into vector pCS2-GFP to express GFP-IMP1/2/3 fusion proteins respectively.

IMP1-5'-EcoR1: AAAAGAATTCGCCGCCACCATGAACAAGCTGTACATCGGGAACC

IMP1-3'-Xba1: AAAATCTAGATTTCCTCCTCGCTTGCAGCTGGCC

IMP2-5'-Sal1: AAAAGTCGACAGATCTATGTGTCCTCCGGATGGGGAATATGC

IMP2-3'-Xba1: AAAATCTAGACCTGCTGGACGATTTCCCTGATCTTGC

IMP2-5'-Xho1: AAAACTCGAGGGCCGGGGGCAGCGCAGCATCGC

IMP2-3'-Xba1-2: AAAATCTAGATTACCCTCTCCTGCTCGGGGGTTCCC

IMP3-5'-EcoR1: AAAAGAATTCGCCGCCACCATGAACAAGCTCTACATCGGCAACCT

IMP3-3'-Xba1: AAAATCTAGATTTTCGTCTTGGCTGAGGCTGTCC

To confirm knockdown by Western blot, because only a fraction of commissural neurons become electroporated in vivo, the shRNAs were tested in cultured cells. 0.8 µg of shRNA plasmids (one control shRNA, two IMP2 shRNAs) and 0.1µg of RFP plasmids were transfected into 293 cells (HEK-293, American Type Culture Collection) in 24 well plates in triplicate using lipofectamine 2000 (Invitrogen). After 24 hours, 0.01 µg of each template plasmid (GFP-IMP1, GFP-IMP2, GFP-IMP3) was transfected separately into previously shRNA-transfected cells. After 48 hours, cells were washed with cold PBS, lysed in 100 µl/well SDS-PAGE sample buffer, and sonicated 30 seconds to shear DNA. Then the lysates were heated at 95°C for 10 min and analyzed by SDS-PAGE and Western blot with anti-GFP antibody (1:1000, Invitrogen A11122).

Characterization of spinal commissural axons by ovo electroporation

In ovo electroporation in chicken embryos was performed essentially as described (Reeber et al., 2008; Avraham et al., 2010). Briefly, fertilized white eggs (Charles River Laboratories)

were incubated at 38°C for 64 hours. DNA mix (1-4 µg/µl) containing IMP2 or control shRNA and Math1-GFP plasmid diluted in 1xPBS and trypan blue solution was introduced with a fine glass micropipet into the spinal cord lumen of HH stage 17 chicken embryos, and unilaterally electroporated into the spinal cord. The Math1-GFP plasmid was constructed by replacing the CMV promoter in the plasmid pCS2-GFP with the Math1 promoter region from Math1-Tau-GFP plasmid, a kind gift from Dr. Jane Johnson (UT Southwestern) (Helms and Johnson, 1998; Lumpkin et al., 2003). Square-wave current (five pulses, 25 V, 50 ms ON and 950 ms interval) was generated using CUY21 electroporator (BEX CO., LTD). Windowed eggs were further incubated at 37°C for 64 hrs, then mounted as open book preparations and imaged by confocal microscopy using a Nikon Ti inverted microscope, equipped with a Yokagawa CSU-10 spinning disk confocal, a Hamamatsu ORCA-AG cooled CCD camera, and Metamorph image acquisition software. Axon numbers were counted at the dorsoventral locations indicated in Fig. 4 by an investigator blind to the shRNA used. Results were tested for statistical significance by Student's unpaired two-tailed t-test, with similar variance between the groups being compared.

To assess the effects of IMP2 RNAi on ROBO1 expression, pmath1-GFP and shRNA plasmids were introduced into the spinal cord of HH stage 17 chick embryos in ovo as described above. 64h after electroporation, commissural neuron cultures were prepared by isolating, and dissociating dorsal spinal cord tissue, followed by culture for 24h on glass coverslips coated with poly-D-Lysine and laminin. Cells were then fixed in 4%paraformaldehyde, 3% sucrose, washed four times with PBS, and incubated with rabbit anti-ROBO1 antibodies (Rockland # 600-401-692) in PBS + 1% BSA + 0.1% Triton X-100 overnight at 4C, washed again as above, incubated 1h at room temperature in Alexa flurophore-conjugated anti-rabbit antibody and phalloidin-rhodamine in PBS + 1% BSA, and mounted in Fluoromount G (SouthernBiotech). Images were captured using a Nikon 80i

upright fluorescence microscope. ROBO1 immunolabeling was quantified using the Metamorph software package. Immunolabeling intensities were measured in cell bodies and growth cones traced with Metamorph based on the phalloidin-rhodamine staining. Neurons were selected for quantitation based on GFP expression, blind to the ROBO1 channel. Fig. 4G displays total axon immunofluorescence; comparable effects on ROBO1 were seen when normalizing by axon area or GFP levels. In micrographs for display (Fig. S4B), contrast and brightness were adjusted for visualization; for quantitation, unadjusted raw images were used with no pixels saturated. Results were tested for statistical significance by Student's unpaired two-tailed t-test, with similar variance between the groups being compared.

All animal experiments were performed in compliance with relevant ethical regulations, and were approved by the IACUC at Harvard Medical School.

SUPPLEMENTAL REFERENCES

Avraham, O., Zisman, S., Hadas, Y., Vald, L., and Klar, A. (2010). Deciphering axonal pathways of genetically defined groups of neurons in the chick neural tube utilizing in ovo electroporation, Journal of visualized experiments : JoVE.

Bailey, T., Boden, M., Buske, F., Frith, M., Grant, C., Clementi, L., Ren, J., Li, W., and Noble, W. (2009). MEME SUITE: tools for motif discovery and searching, Nucleic acids research *37*, 8.

Gumy, L.F., Yeo, G.S., Tung, Y.C., Zivraj, K.H., Willis, D., Coppola, G., Lam, B.Y., Twiss, J.L., Holt, C.E., and Fawcett, J.W. (2011). Transcriptome analysis of embryonic and adult sensory axons reveals changes in mRNA repertoire localization, RNA *17*, 85-98.

Hafner, M., Landthaler, M., Burger, L., Khorshid, M., Hausser, J., Berninger, P., Rothballer, A., Ascano, M., Jungkamp, A.-C., Munschauer, M.*, et al.* (2010). Transcriptome-wide identification of RNA-binding protein and microRNA target sites by PAR-CLIP, Cell *141*, 129-141.

Helms, A., and Johnson, J. (1998). Progenitors of dorsal commissural interneurons are defined by MATH1 expression, Development (Cambridge, England) *125*, 919-928.

Huang, D.W., Sherman, B., and Lempicki, R. (2009). Systematic and integrative analysis of large gene lists using DAVID bioinformatics resources, Nature protocols *4*, 44-57.

Langmead, B., Trapnell, C., Pop, M., and Salzberg, S.L. (2009). Ultrafast and memory-efficient alignment of short DNA sequences to the human genome, Genome Biol *10*, R25.

Licatalosi, D.D., Mele, A., Fak, J.J., Ule, J., Kayikci, M., Chi, S.W., Clark, T.A., Schweitzer, A.C., Blume, J.E., Wang, X.*, et al.* (2008). HITS-CLIP yields genome-wide insights into brain alternative RNA processing, Nature *456*, 464-469.

Lumpkin, E.A., Collisson, T., Parab, P., Omer-Abdalla, A., Haeberle, H., Chen, P., Doetzlhofer, A., White, P., Groves, A., Segil, N.*, et al.* (2003). Math1-driven GFP expression in the developing nervous system of transgenic mice, Gene Expr Patterns *3*, 389-395.

Preitner, N., Quan, J., Nowakowski, D.W., Hancock, M.L., Shi, J., Tcherkezian, J., Young-Pearse, T.L., and Flanagan, J.G. (2014). APC is an RNA-binding protein, and its interactome provides a link to neural development and microtubule assembly, Cell *158*, 368-382.

Reeber, S.L., Sakai, N., Nakada, Y., Dumas, J., Dobrenis, K., Johnson, J.E., and Kaprielian, Z. (2008). Manipulating Robo expression in vivo perturbs commissural axon pathfinding in the chick spinal cord, J Neurosci *28*, 8698-8708.

Tompa, M. (1999). An exact method for finding short motifs in sequences, with application to the ribosome binding site problem, Proceedings / International Conference on Intelligent Systems for Molecular Biology ; ISMB International Conference on Intelligent Systems for Molecular Biology, 262-271.

Trapnell, C., Williams, B., Pertea, G., Mortazavi, A., Kwan, G., van Baren, M., Salzberg, S., Wold, B., and Pachter, L. (2010). Transcript assembly and quantification by RNA-Seq reveals unannotated transcripts and isoform switching during cell differentiation, Nature biotechnology *28*, 511-515.

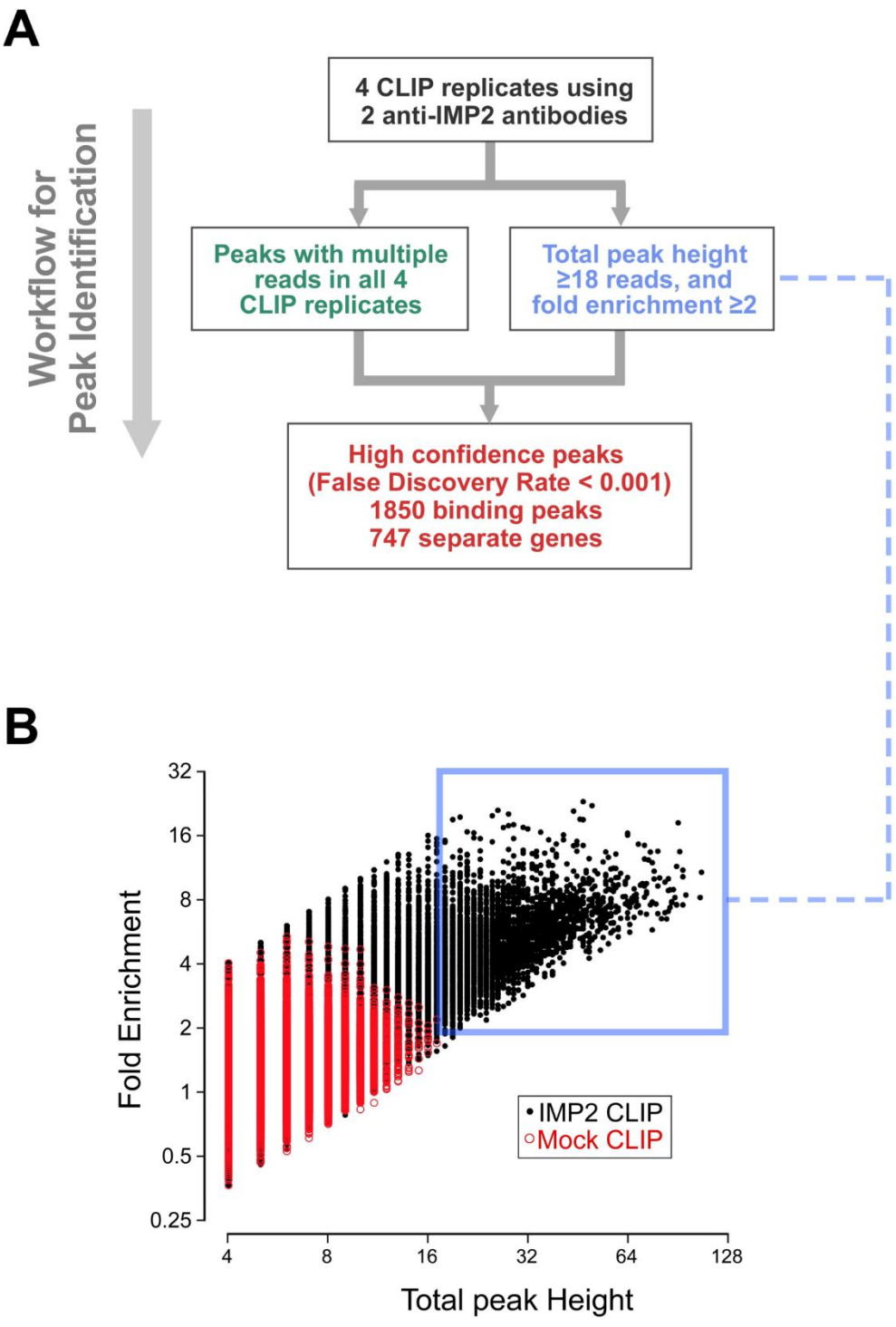

Figure S1. Criteria for selection of high confidence mRNA targets.

(A) Workflow of the analysis. Left box in the flowchart: Only clusters with multiple overlapping reads in all four CLIP replicates were considered: a minimum of four reads in at least three of the four replicates, and a minimum of two reads in the fourth replicate. Right box in the flowchart: For each cluster, reads from all four replicates were pooled and a peak height corresponding to the position of maximum number of overlapping reads within the cluster was calculated. Only peaks with a minimum height of 18, and minimum 2-fold enrichment were further considered based on comparison to the estimated background. **(B)** To estimate background, we generated random samples (mock CLIP), each matching in size the IMP2 CLIP dataset, from control brain mRNA-seq data. A median background number of reads was calculated for each position on the genome, based on repeated sampling of mock CLIP datasets. Enrichment over background (fold change) was then calculated for each cluster, by comparing peak height in IMP2 HITS-CLIP with the median read number of mock CLIP at the corresponding genomic location. Peak height and fold change were then plotted for IMP2 HITS-CLIP as well as for a mock HITS-CLIP sample (lower panel). From this analysis, it was found that choosing a peak height of at least 18, and fold enrichment of at least 2, reduces the false discovery rate to <0.001.

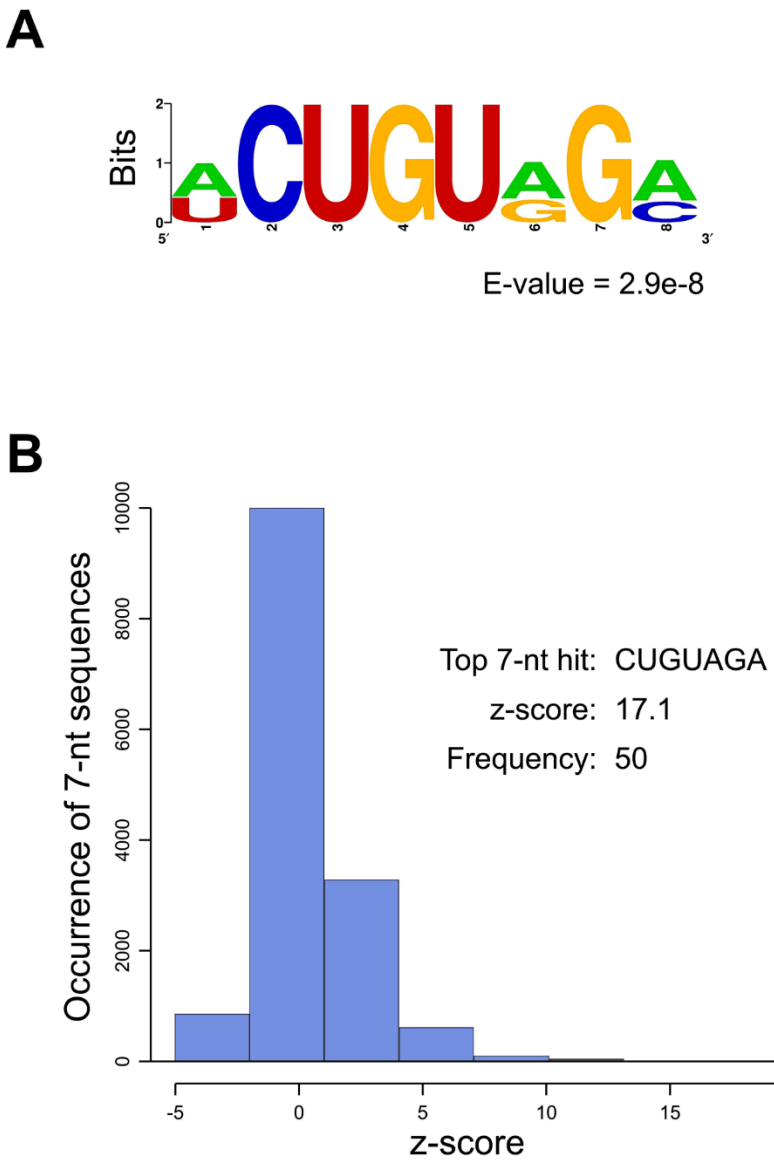

Figure S2. Identification of enriched sequence motif at IMP2 binding sites.

(A) Sequence motif identified by MEME software. (**B)** A preferential binding sequence was also identified using Z-score statistics. Histogram of z-scores indicates the enrichment of 7-nt sequences in all IMP2 CLIP peaks, and the most enriched 7-nt sequence is shown. The two approaches are consistent with one another in identifying an enriched motif. A previous study by Hafner et al. included IMP2 in a validation of the PAR-CLIP approach in cultured HEK-293 cells (Hafner et al., 2010). The use of HITS-CLIP here enabled us to investigate IMP2 mRNA targets in native brain, to identify targets relevant to neural development. Also, this approach assesses native IMP2 (endogenous levels and isoforms), whereas the previous approach used recombinant IMP2 in an overexpression system which can result in formation of aberrant complexes of IMP proteins (Bell et al., 2013).

Disease Associations

Disease clusters	Disease terms	*p*
Psychiatric	Schizophrenia	2e-11
Neurodegeneration	Amyotrophic lateral sclerosis Huntington's disease Alzheimer's disease Parkinson's disease	4e-9 3e-8 4e-6 7e-3
Brain cancer	Glioblastoma Astrocytoma Glioma	3e-8 4e-8 1e-7
Neurodevelopment	Type 1 Lissencephaly Mental retardation	2e-6 2e-4
Other	Gliosis	4e-3

Figure S3: IMP2 target mRNAs encode proteins linked to neurologic diseases.

Associated disease terms were identified by IPA Disease and Disorder Analysis (see Materials and Methods).

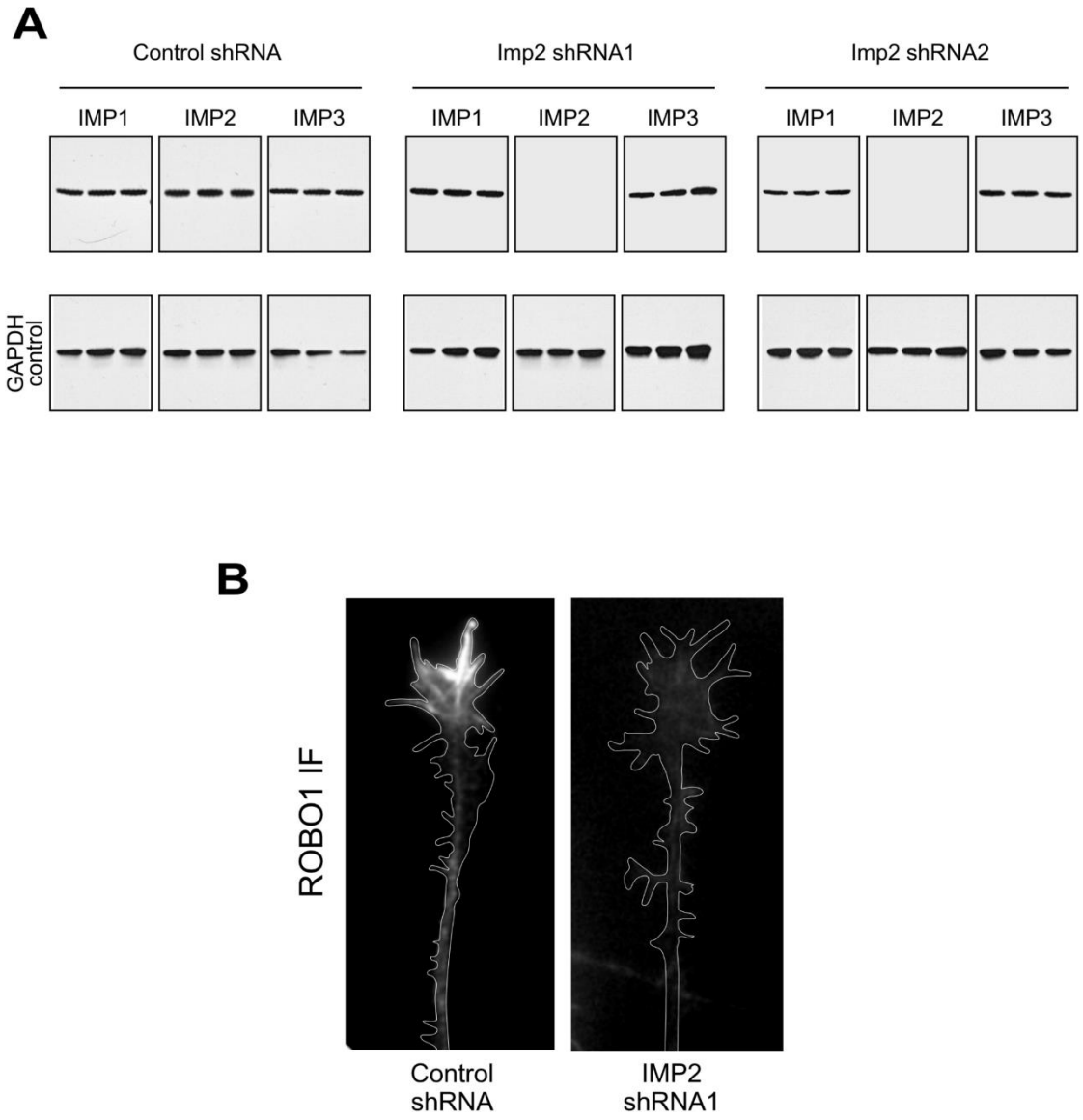

Figure S4: Confirmation of protein knockdown by IMP2 shRNAs, and reduced expression of the IMP2 target *Robo1* on axons. **(A)** Western blot, confirming that two independent IMP2 shRNAs strongly knocked down protein expression from IMP2 mRNA, compared with controls including IMP1 and IMP3 mRNAs, and the metabolic housekeeping enzyme GAPDH. **(B)** ROBO1 immunofluorescence was reduced on commissural axons after in vivo treatment with IMP2 shRNA compared with control shRNA. To visualize individual axons, immunolabeling was performed after dissociating the neurons and placing them in culture. A white line indicates the outer boundary of the growth cone and distal axon shaft based on phalloidin-rhodamine labeling.

Table S1

Click here to Download Table S1

Table S2

Click here to Download Table S2